

Compressive sampling in passive millimeter-wave imaging

N. Gopalsami*¹, T. W. Elmer¹, S. Liao¹, R. Ahern¹, A. Heifetz¹, A. C. Raptis¹
M. Luessi², D. Babacan², and A. K. Katsaggelos²

¹Nuclear Engineering Division, Argonne National Laboratory,
9700 S. Cass Avenue, Argonne, IL, 60439;

²Department of Electrical Engineering and Computer Science, Northwestern University,
2145 Sheridan Road, Evanston, IL 60208

ABSTRACT

We present a Hadamard transform based imaging technique and have implemented it on a single-pixel passive millimeter-wave imager in the 146-154 GHz range. The imaging arrangement uses a set of Hadamard transform masks of size $p \times q$ at the image plane of a lens and the transformed image signals are focused and collected by a horn antenna of the imager. The cyclic nature of Hadamard matrix allows the use of a single extended 2-D Hadamard mask of size $(2p-1) \times (2q-1)$ to expose a $p \times q$ submask for each acquisition by raster scanning the large mask one pixel at a time. A total of $N = pq$ acquisitions can be made with a complete scan. The original $p \times q$ image may be reconstructed by a simple matrix operation. Instead of full N acquisitions, we can use a subset of the masks for compressive sensing. In this regard, we have developed a relaxation technique that recovers the full Hadamard measurement space from sub-sampled Hadamard acquisitions. We have reconstructed high fidelity images with 1/9 of the full Hadamard acquisitions, thus reducing the image acquisition time by a factor of 9.

Keywords: Passive, millimeter wave, compressive sensing, Hadamard transform

1. INTRODUCTION

Compressive sensing (CS) with single-pixel imaging involves exploiting the sparsity or compressibility of the image matrix such that one can make fewer measurements (less samples) than what is dictated by the Nyquist limit, yet the image can be reconstructed with high fidelity [1]. CS-based image acquisition measures the inner product of the scene and a test function with a single-pixel sensor. The test function is a mask of random weighting parameters acting on the scene pixels to provide a set of incoherent measurements. It has been shown that high fidelity images can be reconstructed from compressively sampled image data using advanced reconstruction algorithms [2-3]. CS has been implemented at optical wavelengths by taking advantage of digital micromirror devices (DMD) for electronic generation of random masks. The CS implementation at millimeter wavelength, however, is not straightforward due to a lack of suitable spatial intensity modulators such as DMMs. CS-based imaging has been implemented on a single-pixel active terahertz imaging system using random masks made of copper tapes on plastic plate [4]. These masks were introduced manually one at a time to prove feasibility.

Long before the appearance of CS, Hadamard transform imaging has been in use for coded-aperture gamma-ray imaging where the traditional lens imaging is not practical [5]. It is efficient in the presence of noise and the implementation is similar to that of CS for a full set of image acquisitions [6]. Due to the incoherent nature of the blackbody emission, the detected intensity for each realization in the Hadamard space can be considered as a linear summation of the 0 or 1 weighted image; as a result, its SNR is higher than that by scanning with a single aperture. It also allows subwavelength pixel size for image resolution. The original image can be reconstructed by inverse transforming the set of Hadamard mask collected data [6]. We present in this paper a Hadamard mask-based millimeter wave image acquisition technique with subwavelength pixel size and a real-time image reconstruction method in which a subset of the Hadamard measurement space is used to speed up the image acquisition as in CS.

*gopalsami@anl.gov; phone: 630.252.5925; fax: 630.252.3250

2. HADAMARD TRANSFORM IMAGING

Figure 1 shows a single-pixel passive millimeter-wave setup for Hadamard transform imaging. An incandescent 60W light bulb is used as an illumination source. For the target to be imaged, we used a 2.54cm diameter circular hole in a 10cm \times 10cm metal plate along with a 3mm wide rectangular strip pasted across the hole. An extended Hadamard mask is raster scanned in front of the scene, and the illuminated radiation through each mask position and scene is collected by a 2.54cm diameter dielectric lens and fed to a 146-154 GHz Dicke-switched radiometer.

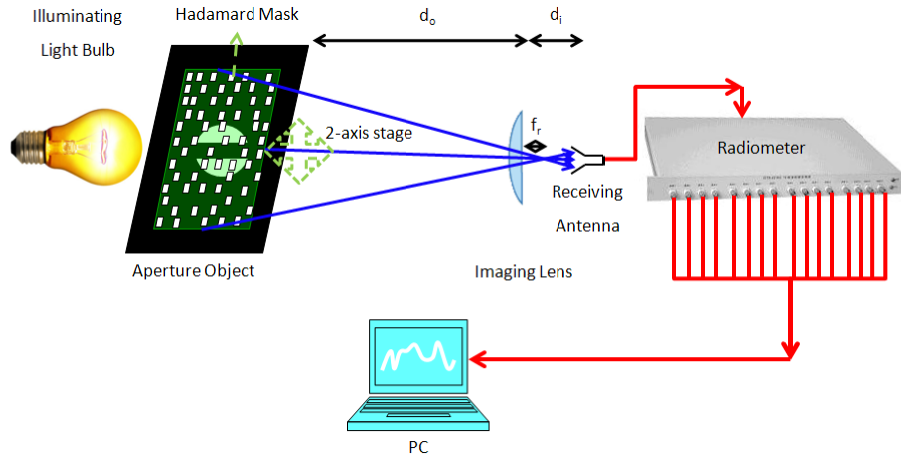


Figure 1. Hadamard transform imaging system: a light bulb illuminates a scene comprised of a 2.54cm diameter circular hole with a 3mm wide rectangular metal strip, which is encoded by the Hadamard mask in front of the scene; the encoded scene is focused on and collected by the receiving antenna for each mask position exposing 41×43 pixels.

Figure 2(a) gives the layout of the extended 2D Hadamard mask; it is realized by periodically extending a cyclic S -matrix with $pq \times pq$ elements (based on twin-prime construction [6]) and folding the elements of the first row of the S -matrix into a $p \times q$ matrix. We used $p = 41$ and $q = 43$ with a pixel size of 1.24 mm to produce 10.04cm \times 10.53cm extended mask with 81×85 pixels. The mask is fabricated using chrome coating on a millimeter-wave transparent quartz plate (Fig. 2(b)).

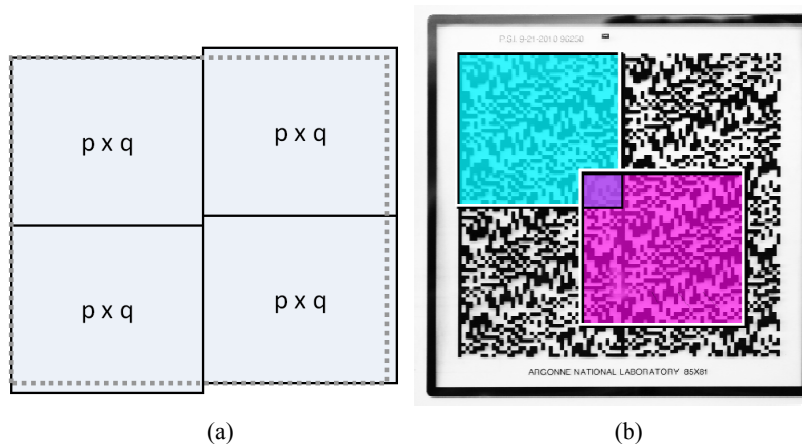


Figure 2. An extended Hadamard mask of size 81×85 pixel: (a) layout and (b) fabricated on a quartz plate with chrome coating. A 41×43 pixel mask area is exposed for each acquisition.

The 2D Hadamard mask is raster scanned by a 2-axis translation stage controlled by a LabVIEW™ program running on a Personal Computer (PC); the transmitted field through the Hadamard mask is focused to the imaging plane of a 2.54cm

diameter imaging dielectric lens (focal length $f_r = 2.54$ cm), where a corrugated circular conical horn antenna is located as part of the radiometer. The lens equation, $1/f_r = 1/d_i + 1/d_o$, should be followed closely for positioning of mask and detector with respect to the lens, where for the object (mask) distance is $d_o = 12.7$ cm, the image distance becomes $d_i = 3.175$ cm. A 146 GHz to 154 GHz radiometer collects Dicke-switched signals over 16 channels which may be used for imaging and spectroscopy [7]. For imaging, we averaged all the channels to increase the SNR.

3. IMAGE RECONSTRUCTION

The received intensity vector $\bar{I}(pq \times 1)$ in Hadamard transform may be expressed as

$$\bar{I}(pq \times 1) = \bar{S}(pq \times pq)\bar{I}_i(pq \times 1), \quad (1)$$

where $\bar{S}(pq \times pq)$ is the cyclic S -matrix realized by the Hadamard mask and $\bar{I}_i(pq \times 1)$ is the scene intensity vector, which can be reconstructed for a full set of Hadamard measurements as follows

$$\bar{I}_i(pq \times 1) = \bar{S}^{-1}\bar{I}(pq \times 1) = \frac{2}{pq+1}(2\bar{S}^T + \bar{J}_{pq})\bar{I}(pq \times 1), \quad (2)$$

where \bar{J} is an all-one matrix. For a given size Hadamard mask, the matrix values in Eq. (2) are predetermined from the Hadamard sequence; as a result, the image reconstruction can be done in real time.

3.1 Full Hadamard reconstruction

Although the transmission through individual pixels suffers for small pixel sizes relative to the wavelength ratio [8], the overall transmission through the mask as used in our setup is not affected significantly as the signals from nearly half of the open mask pixels are summed up by the detector. To analyze the effect of mask on signal contrast, we conducted a signal-to-noise ratio analysis with and without the mask in the imaging setup. We measured first the radiometer signals for three backgrounds: the lamp, liquid nitrogen load, and ambient temperature absorber, without and with the mask in beam path as in Figs. 3(a) and 3(b), respectively. The brightness temperature of the lamp as calibrated with liquid nitrogen and ambient loads is about 475K. The SNR values of the radiometer for the lamp radiation without and with the mask in the beam path are 13.1 and 7.9, respectively (see Fig. 3(c)). A factor of 2 reduction in SNR is a tradeoff for the higher image resolution achieved with subwavelength pixel size.

We first simulated the Hadamard transform for our imaging object – a circular hole with strip across in the middle. Figure 4(a) gives the binary coded image of the object, and Fig. 4(b) its Hadamard transformed image. In this idealized case, the reconstructed image was identical to Fig. 4(a).

We next obtained a full set of 1763 Hadamard acquisitions with our setup in Fig. 1. Figure 5(a) gives the Hadamard transformed image and Fig. 5(b) the reconstructed image. A remarkable agreement is seen between the simulated (Fig. 4(b)) and experimental (Fig. 5(a)) Hadamard transform images. The reconstructed image of a circular hole with a horizontal metal strip shows the feasibility of Hadamard imaging at millimeter wavelength with subwavelength resolution (1.24 mm pixel size for 2 mm wavelength).

3.2 Sub-sampled Hadamard acquisitions and image reconstruction

To get full Hadamard acquisitions, we scanned the extended mask one pixel at a time along q pixels horizontally and p pixels vertically. The number of acquisitions can be reduced if we scan the mask every m^{th} pixel along horizontal and vertical directions. This represents sub-sampled data in the Hadamard transform space. To reconstruct the image, the missing data in the Hadamard space may be calculated with a procedure known as the relaxation method in numerical methods, e.g., 2D solution of Poisson equations in electrostatics [9]. It is an iterative scheme where a trial value at a missing pixel may be obtained as a weighted average of the values at the surrounding pixels. The iterative procedure continues until the predicted values converge. Once the missing pixel values are calculated, the reconstruction matrix in Eq. (2) may be used for image reconstruction.

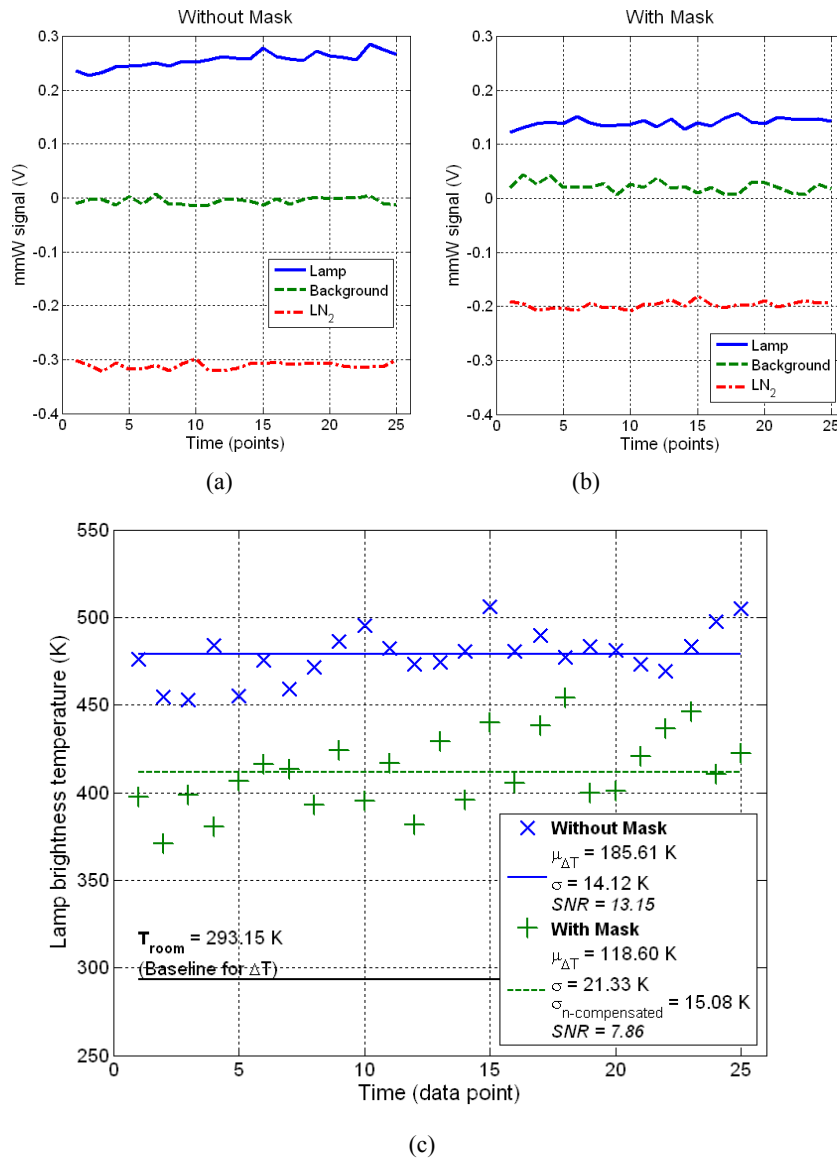


Figure 3. Analysis of signal-to-noise ratios with and without the Hadamard mask: radiometer signals for different backgrounds without (a) and with (b) the mask; (c) lamp brightness temperature without and with the mask. The transmission through mask assumes 50% of the pixels are blocked, and SNR is defined as $\mu_{\Delta T}/\sigma$.

To test the relaxation technique, we sampled every 3rd column and 3rd row of the Hadamard space, providing 1/9 of the Hadamard matrix acquisitions. Figure 6(a) gives the recovered image in Hadamard space, and Fig. 6(b) the reconstructed image of the object. The recovered Hadamard image (Fig. 6(a)) from partial data compares well with the full Hadamard image in Fig. 5(a). Also, the reconstructed image of the object clearly shows the circular hole with a strip across.

If the reconstructed image turns out to be of poor quality, one may sequentially acquire an additional cycle of samples over the missing locations in the Hadamard sampling scheme till satisfactory image quality is obtained. The relaxation method is applied after each cycle of sampling on the Hadamard space, and the image reconstruction can be done in real time as the same matrix operation is used for inversion.

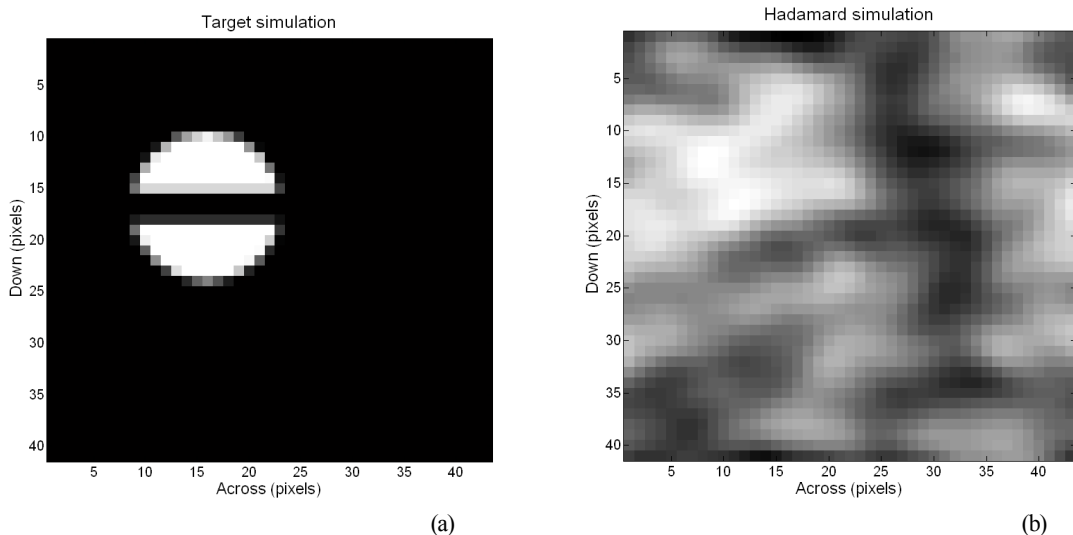


Figure 4. Simulation of target geometry: (a) digitized image of circular hole with a strip across and (b) simulated Hadamard transformed image.

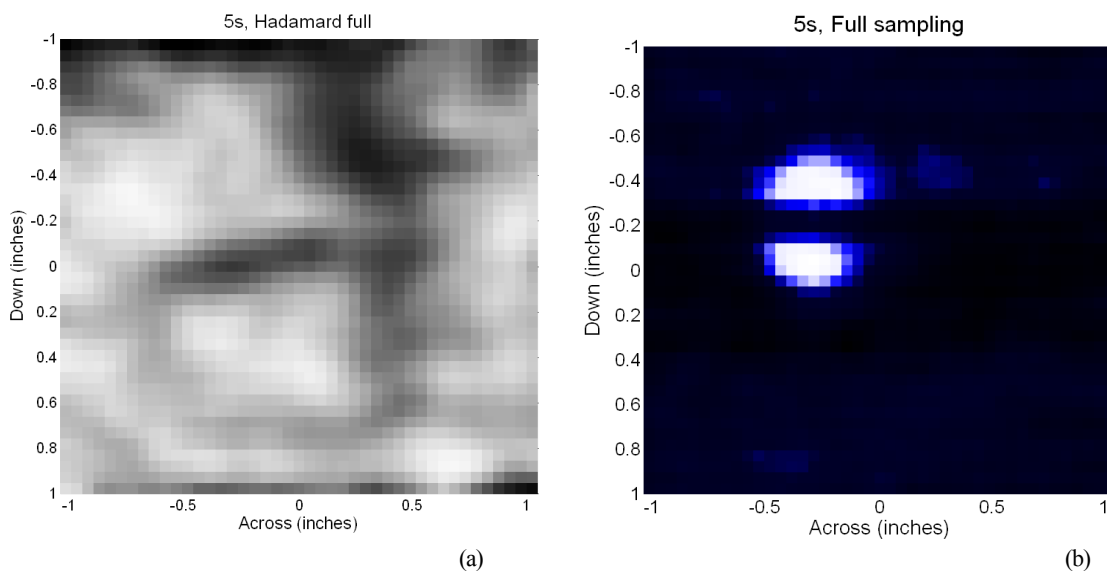


Figure 5. Experimental data: (a) Hadamard transformed image and (b) Reconstructed image.

4. CONCLUSIONS

We have developed a compressive sensing approach for passive millimeter wave imaging application. We used a Hadamard mask of 41×43 pixels, with pixel size of 1.24 mm, about half the wavelength at the center frequency of our 146 GHz to 154 GHz radiometer. An incandescent lamp of brightness temperature 475K was used as an illumination source. An imaging object was placed behind the mask. Single-pixel image acquisitions were obtained by raster scanning an extended cyclic Hadamard mask of 81×85 pixels, which exposes each time a 41×43 image size. The signal to noise ratios of radiometer signals for lamp radiation without and with the Hadamard mask in the beam path were 13.1 and 7.9, respectively; the degradation is not severe considering subwavelength pixels used in the mask. Images were reconstructed for simulated, full (1763) and partial (210) measured acquisitions. The agreement between the simulated and measured Hadamard transform images was very good. In the case of partial acquisitions, we used a

relaxation method to iteratively calculate the missing data in the Hadamard measurement space. The reconstructed image of the object from partial acquisitions ($1/9^{\text{th}}$ of full) compared well with the original image, hence showing the feasibility of this approach for compressive sampling.

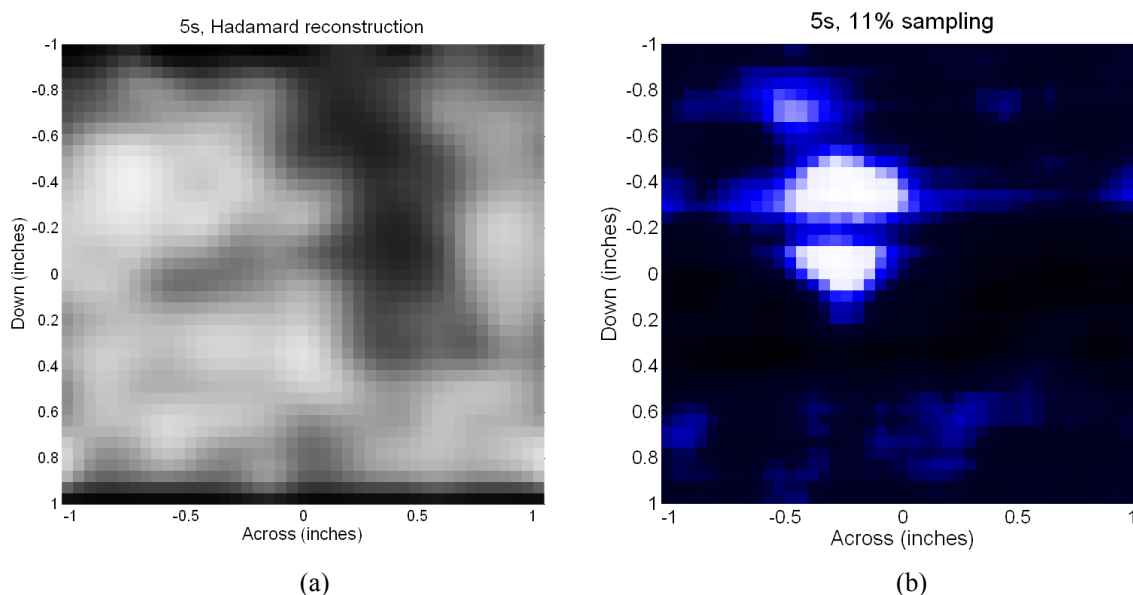


Figure 6. Reconstructed image from $1/9^{\text{th}}$ of samples: (a) relaxation-based Hadamard space reconstruction and (b) reconstructed image of the scene.

Acknowledgements

The work at Argonne is supported by the office of Nonproliferation and Verification Research and Development under the National Nuclear Security Administration of the U.S. Department of Energy under Contract No. DE-AC02-06CH11357. The work at Northwestern University is supported in part by a grant from the U.S. Department of Energy DE-NA0000457.

REFERENCES

- [1] Donoho, D. L., "Compressed sensing," IEEE Transaction on Information Theory, Vol. 52, 1289-1306 (2006).
- [2] Duarte, M. F., Davenport, M. A., Takhar, D., Laska J. N., Sun T., Kelly K. F., Baraniuk R. G., "Single-pixel imaging via compressive sampling", IEEE Signal Processing Magazine, 83-91 (2008).
- [3] Baraniuk, R.G., "Compressive sensing," IEEE Signal Processing Magazine, Vol. 24, No. 4, 118-120 (2007).
- [4] Chan, W.L., Charan, K., Takhar, D., Kelly, K.F., Baraniuk, R.G., Mittleman, D.M., "A single-pixel terahertz imaging system based on compressive sensing," Applied Physics Letters, 93, 121105 (2008).
- [5] Stephen, J.B., "Techniques of Coded Aperture Imaging for Gamma-Ray Astronomy," Adv. Space Res. 11, (8)407-(8)418, 1991.
- [6] Harwit, M., Sloane, N. [Hadamard Transform Optics], Academic Press, New York (1979).
- [7] Gopalsami, N, Liao, S., Koehl, E. R., Elmer, T. W., Heifetz, A., Chien, H. T., Raptis, A. C., "Passive Millimeter Wave Imaging and Spectroscopy System for Terrestrial Remote Sensing," Proc. of SPIE, vol. 7670, pp. 767003-1:767003-7 (2010).
- [8] Lynch, J, Matic, R., Baron, J., "Performance Limitations of Compressive Sensing for Millimeter wave Imaging," Proc. of SPIE, vol. 7670, pp. 76700D-1:76700D-8 (2010).
- [9] Jackson, J.D. [Classical Electrodynamics], Wiley, New York (1998).